JOURNAL OF GEOPHYSICAL RESEARCH, VOL. 90, NO. A1, PAGES 359-369, JANUARY 1, 1985

Precipitation of Radiation Belt Electrons by Man-Made Waves: A Comparison Between Theory and Measurement

U. S. INAN, H. C. CHANG, AND R. A. HELLIWELL

STAR Laboratory, Stanford University, California

W. L. IMHOF, J. B. REAGAN, AND M. WALT

Lockheed Palo Alto Research Laboratory, Palo Alto, California

The temporal and spectral shape and the absolute flux level of particle pulses precipitated by a VLF transmitter are examined from a theoretical point of view. A test-particle model of the gyroresonant wave-particle interaction is applied to the parameters of the observed cases for calculating the precipitation characteristics. The temporal shapes of the precipitation pulses are found to be controlled (1) by the pitch angle dependence of the particle distribution near the edge of the loss cone and (2) by the multiple interaction of the particles with the waves due to significant atmospheric backscatter.

1. INTRODUCTION

The precipitation of radiation belt electrons as a result of resonant interactions with waves is an important mechanism for the transfer of energy from the magnetosphere to the ionosphere. One-to-one correlations between natural VLF waves (whistlers, emissions) and ionospheric effects (X rays, photoemissions, density enhancements, amplitude and phase changes of subionospheric VLF signals) have been attributed to wave-induced precipitation [*Rosenberg et al.*, 1971; *Helliwell et al.*, 1973, 1980; *Larsen et al.*, 1976; *Arnoldy et al.*, 1982; *Dingle and Carpenter*, 1981]. Application of a theoretical test-particle model of the gyroresonant wave-particle interaction to some of the observed cases has provided support for the hypothesis that the observed ionospheric effects are the result of wave-induced scattering of electrons into the bounce loss cone [*Inan et al.*, 1982; *Chang and Inan*, 1983].

Observations of the energy spectra of electrons in the drift loss cone, where narrow resonant peaks were attributed to precipitation induced by ground based transmitters [*Imhof et al.*, 1974, 1981; *Vampola and Kuck*, 1978; *Koons et al.*, 1981], have provided the first evidence of the possibility of detecting precipitation resulting from interactions with man-made waves. More recently, precipitation of radiation belt electrons by VLF waves injected under program control from ground based transmitters was achieved during the Stimulated Emission of Energetic Particles (SEEP) experiments [*Imhof et al.*, 1983*a*, *b*]. These results constitute the first direct satellite based observations of modulated precipitation of electrons in the bounce loss cone. In addition, rocket based observations of X rays during modulated injection of VLF waves were attributed to transmitter induced precipitation [*Goldberg et al.*, 1983].

Paper number 4A8162.
0148-0227/85/004A-8162$05.00

In this paper we consider the temporal and spectral shape as well as the absolute flux level of the precipitation pulses observed directly on the satellite [*Imhof et al.*, 1983*a*]. In order to reproduce these observations by theoretical modeling, we find it necessary to consider both the pitch angle dependence of the particle distribution near the edge of the loss cone as well as atmospheric backscatter which leads to multiple interactions of the particles with the wave.

2. REVIEW OF OBSERVATIONS

Of the five different modulated electron flux events reported [*Imhof et al.*, 1983*b*], the one observed on August 17, 1982, was outstanding in terms of both the L range of observations and the ratio of peak flux to background level. It was concluded however, that most features of the observed precipitation pulses were similar in all the reported cases [*Imhof et al.*, 1983*a*, *b*]. In the following we summarize some of the basic features of the August 17, 1982, case:

1. Peaks in the energy spectrum of precipitating electrons were observed from L=2.1 to 2.4 (a distance of $\sim$ 500 km at the satellite altitude of $\sim$ 220 km). The energy at which the peak occurred was found to depend on L, being equal to 17.7 keV at L=2.3. Assuming gyroresonant interactions at or close to the magnetic equator, the variation with L was consistent with an L^{-4} dependence of n_{eq}, the equatorial cold plasma density. The peak count rate increased by a factor of $\sim$4 from L=2.1 to 2.3 but decreased rapidly for $L > 2.4$.

2. The rise time of the flux was longer by an additional $\sim$1.5 seconds than that to be expected on the basis of $t_w + t_e$, where t_w and t_e are respectively the wave travel time to the equator and the particle travel time from the equator to the satellite altitude. (As shown in the appendix, $t_w \simeq 0.2$-0.4 s for a 17.8 kHz wave and $t_e \simeq 0.2$ s for 17.7 keV particles at $L \simeq 2.3$.) This rise time is illustrated in Figure 1 which duplicates Figure 2*a* of *Imhof et al.*, 1983*a*. The solid line shows the precipitation pulse shape obtained by superposed epoch analysis on 8 consecutive pulses. The dotted line indicates the flux-versus-time profile predicted by a first order

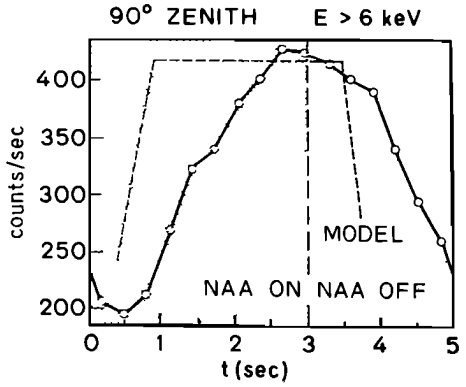

Fig. 1. Taken from Figure 2 of *Imhof et al.* [1983a], this figure shows the superposed epoch average of eight consecutive precipitation pulses observed during August 17, 1982. The dotted line shows the flux-versus-time profile predicted by application of the *Inan et al.*, 1982 model to the parameters of this case, omitting backscatter and multiple interactions of particles with the wave.

(assuming no backscatter, no multiple interactions with the wave and a sharp loss cone edge) application of the wave-induced precipitation process to the parameters of this case [*Inan et al.*, 1982]. The predicted flux reaches its peak value in a time equal to $t_w + t_e \simeq 0.7$ seconds. The peak flux is sustained for the duration of the wave pulse (3 seconds) and then decreases. With this theory there is no significant change in the flux level as long as the wave pulse is in the vicinity of the geomagnetic equator.

3. The observed decay of the flux showed an unexpected delay of ~1.5 s; i.e., the precipitation pulse extended beyond the time at which the particles resonating with the wave tail at the equator should have arrived at the satellite altitude.

In the following we explain the observed pulse shapes as a result of multiple encounters of the particles with the wave during successive particle bounces.

3. Conceptual Basis for a Model of the Observed Events

Since the bounce period for 17.7 keV particles near the loss cone at $L \simeq 2.3$ is equal to $\tau_B = 4t_e \simeq 0.78$ seconds, it is possible for a given particle to encounter the wave 3-4 times during the 3 second duration of the pulse. In such a case, the particles might move down into the loss cone in two or more steps, so that the precipitation flux reaches a maximum a few τ_B (0.78 s) later than expected. This change is in the right direction to explain the observed ~ 1.5 s additional delay, but the situation is complicated by the difference in the northern and southern mirror altitudes.

As a result of the South Atlantic anomaly, there exists an asymmetry in the earth's magnetic field intensity between the two conjugate hemispheres. At $L \simeq 2.3$ and at the longitude of the NAA transmitter, the difference in particle mirror heights is ~300 km [*Olson et al.*, 1979]. Thus the southern hemisphere mirror point for the particles observed by the SEEP detector at ~220 km altitude in the northern hemisphere is below sea level. This north-south asymmetry

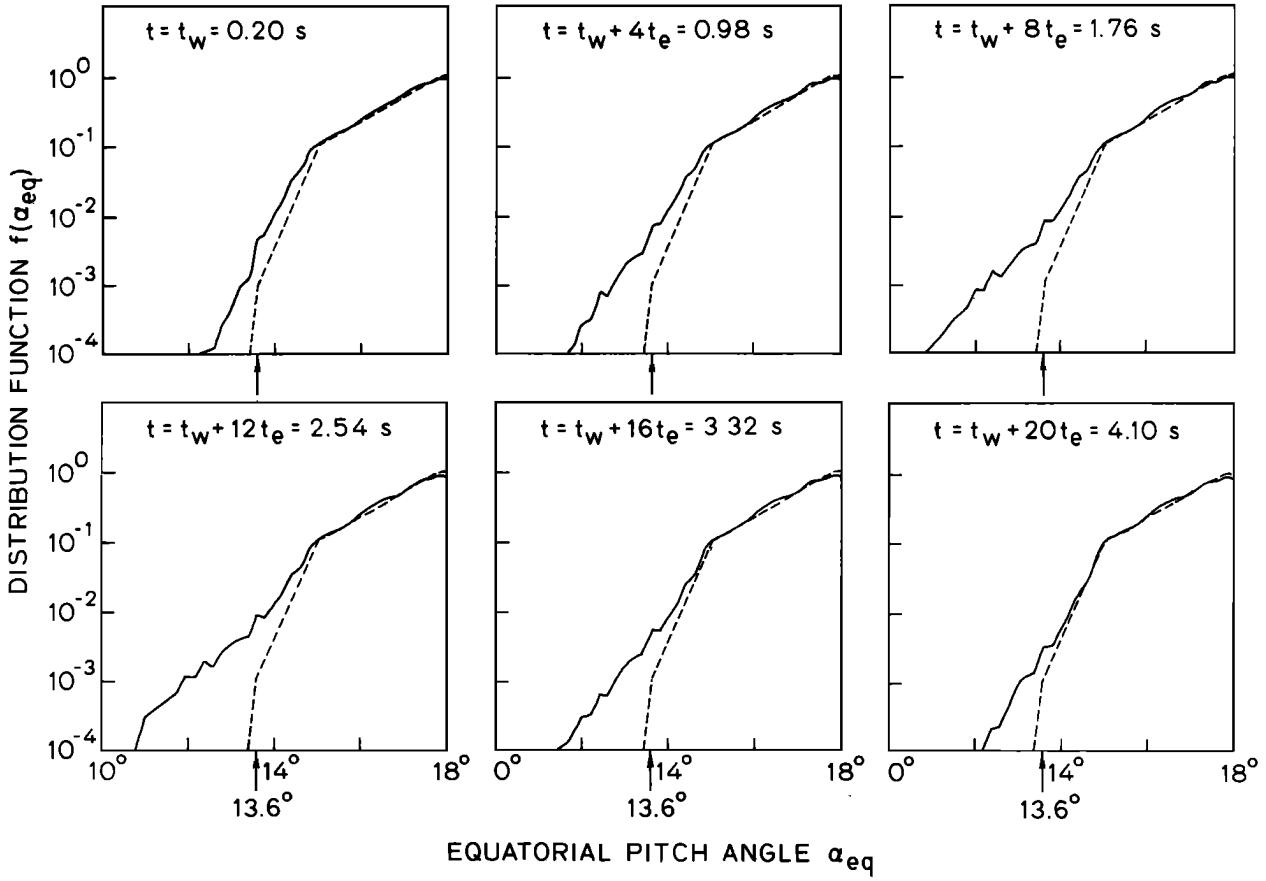

Fig. 2. The evolution of the energetic particle distribution. The distributions $f(\alpha_{eq})$ versus α_{eq} are shown at various instants of time. The result shown is for B_w=15 pT and for an initial distribution shown in dashed lines.

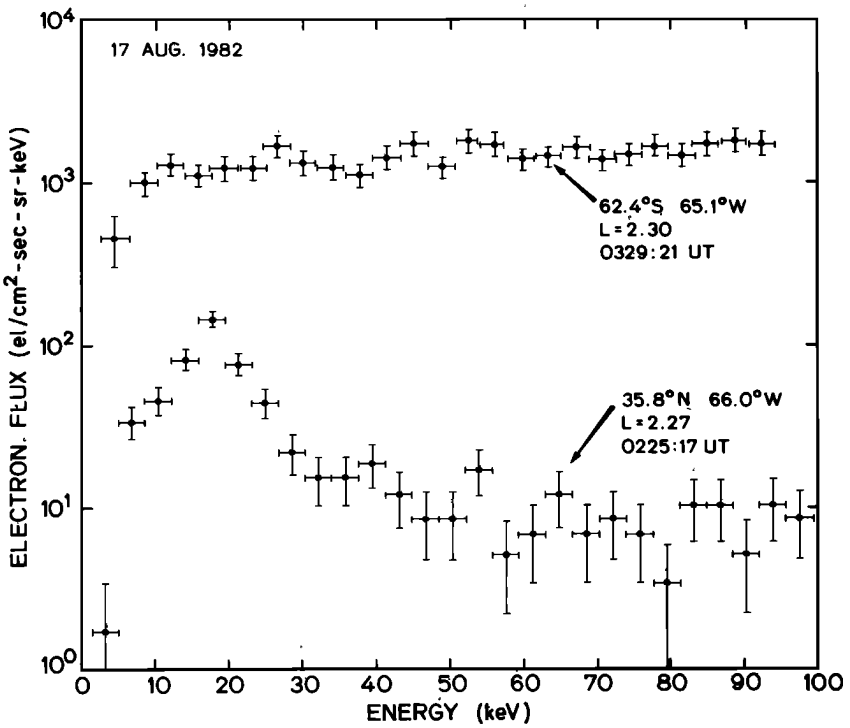

Fig. 3. The lower set of points show the differential energy spectrum measured in the northern hemisphere during the time of observation of the NAA modulated fluxes. The result shown is from the detector with a central zenith angle of 90°. The upper points show the same quantity measured with the same detector in the southern hemisphere during the next orbit near the same longitude. The fluxes shown are obtained by averaging over a 1.95 second period starting at the indicated UT times.

of the geomagnetic field can also be expressed in terms of the equatorial loss-cone angle (α_{lc}) corresponding to a fixed mirror height in a particular hemisphere. For the present case, the southern and northern equatorial loss cone angles differ by as much as 2°. Specifically, for an altitude of $\sim$ 100 km $\alpha_{lc}^{S} = 15°$ whereas $\alpha_{lc}^{N} = 13°$ [*Olson et al.*, 1979]. The SEEP detectors in the northern hemisphere at $\sim$220 km altitude observe particles with equatorial pitch angles $\alpha_{eq} \leq 13.6°$, where 13.6° is the equatorial pitch angle corresponding to a local pitch angle of 90° at the satellite altitude.

In view of the above, any particles observed by the SEEP detectors must have been scattered from a pitch angle $\alpha_{eq} \geq 15°$ to $\alpha_{eq} \leq 13.6°$ during the last half bounce of the particle. Any particle scattered less than 1.4° would fall in the range $13.6° < \alpha_{eq} < 15°$ and would thus mirror at an altitude above that of the SEEP satellite in the north. Such particles would be precipitated in the southern hemisphere and would not contribute to the flux observed by the SEEP detectors unless backscattered by the atmosphere.

In order for a particle with an initial $\alpha_{eq} > 15°$ to be scattered to a pitch angle below 13.6° in two or more steps, one of two processes must occur. In one case, the single encounter scattering $\Delta\alpha_{eq}$ of an individual particle may exceed 1.4°, so that particles may be scattered first to the vicinity of 15° and then across the gap to a pitch angle $\alpha_{eq} < 13.6°$. In the second case, individual $\Delta\alpha_{eq}$ can be smaller, so that particles may have pitch angles in the range $13.6° < \alpha_{eq} < 15°$ in between successive wave-induced scatterings. However, in the latter case, atmospheric backscatter in the southern hemisphere of a significant percentage of such particles is necessary in order for this class of particles to contribute to the observed fluxes in the north.

The second case described above combined with atmospheric backscatter would be consistent with the observed delay in the decay of the flux, i.e., the persistence of the flux beyond the time $t = t_e + t_w + t_P$, where t_P is the wave pulse duration. The flux observed beyond this time t would be due to particles with pitch angles $\alpha_{eq} \leq 13.6°$, some of which would backscatter from the northern and southern hemispheres and thus would be observed by the SEEP detector again.

Interaction of precipitating electrons with the atmosphere has been studied by several authors [e.g., *Stadsnes and Maehlum*, 1965; *Berger et al.*, 1974; *Davidson and Walt*, 1977]. These theoretical calculations indicate that the fractional number of particles that backscatter from the atmosphere increases with local pitch angle. Thus, for particles that impinge on the atmosphere with grazing pitch angles, as would be the case for wave-induced scattering near the vicinity of the equatorial loss cone, the fractional atmospheric backscatter can be as high as 80-90%.

While the waves that scattered the electrons observed by SEEP on August 17, 1982, were probably propagating in the nonducted mode (see appendix), in estimating the wave-induced scatterings, we consider only a longitudinally (θ=0°) propagating wave. For nonducted interactions, wave-induced scattering would be dependent on the particular configuration of ray paths in the magnetosphere, which in turn depend on the background cold plasma density profile [*Bell*, 1984]. In general, the location of maximum interaction for the nonducted case may be off the magnetic equator. On the other hand, at least for a relatively smooth distribution of ray paths, we expect the temporal variation of the precipitated flux to be similar for ducted and nonducted waves.

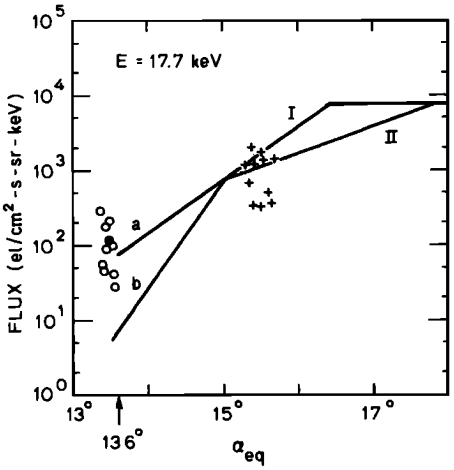

Fig. 4. The differential flux of 17.7 keV particles at $L \simeq 2.3$ measured at the southern and northern hemisphere on the SEEP satellite on different passes during the month of August 1982 and in the geographic longitude range within ±5° of the NAA transmitter. The data shown represent fluxes averaged over an 8.19 sec period. The pluses and circles correspond to southern and northern hemisphere observations, respectively. The solid circle represents the value measured during the August 17, 1982, event. All data points correspond to the counts measured with the detector at a local zenith angle of 90°. The different loss-cone distributions used in our model calculations are shown in solid lines for comparison.

In the next section we use a modified test particle model of the wave particle interaction [*Inan et al.*, 1982] to calculate the expected characteristics of the precipitation flux. We include multiple encounters between the particles and the waves and backscatter from the atmosphere. The computed results are compared with observations in section 5.

4. Description of the Model

The test-particle model [*Inan et al.*, 1982] numerically evaluates the deflection of electrons which encounter a longitudinally propagating whistler mode wave in the dipole geomagnetic field. This model has previously been used to calculate the intensity, energy spectra and temporal signatures of particle fluxes that would be induced by gyroresonance interactions with monochromatic, longitudinally propagating whistler mode waves in the magnetosphere [*Inan et al.*, 1982]. As outlined above, we now extend the model to allow particles that are scattered into the loss cone in the first encounter with the wave to undergo atmospheric backscatter and multiple interactions with the wave. For the background cold magnetoplasma we use a centered dipole model of the earth's magnetic field and a diffusive equilibrium model for the cold plasma distribution along the field lines. We carry out an iterative calculation in which the perturbed particle distribution function from the previous step is used as the initial distribution for the next step. For the initial distribution at the first step, we consider functions with various pitch angle shapes in the vicinity of the loss cone, as illustrated in later figures. The "loss cone" angles in both hemispheres are chosen on the basis of a mirror altitude of ~100 km.

Although the particles are scattered in pitch angle and energy as a result of their interaction with the atmosphere, in simulating atmospheric backscatter we assume that the backscattered particles do not change energy or pitch angle. We take the fractional number of particles backscattered to be given by $(1-\cos\alpha)$, where α is the local pitch angle of the particle as it enters the atmosphere. This assumed variation closely approximates results obtained by *Berger et al.*, [1974] for the fractional population of particles reflected from the atmosphere. Note that when atmospheric backscatter in the northern and southern hemispheres is considered, the difference in the relationship between α_{eq} and α (i.e., $\alpha_{lc}^S > \alpha_{lc}^N$) must be taken into account.

5. Results

We now present results for the evolution of the energetic particle distribution and the temporal variation of electron flux as it would be observed at the satellite altitude of ~ 220 km in the northern hemisphere. We consider the case of a 3-second long (t_P = 3 s) 17.8 kHz wave pulse propagating longitudinally at L=2.3, where the equatorial electron density is taken to be n_{eq} = 1585 el/cm ^{3} (see appendix). We consider particles with energy 17.7±1.8 keV, since 17.7 keV is the observed energy of the peak at L=2.3 [*Imhof et al.*, 1983*a*] and 3.6 keV is the resolution of the detector. For the cases shown in Figures 3-7 we assume equatorial wave magnetic field intensities of alternatively 15 or 30 pT. As discussed in the appendix, these values are representative of expected intensities for this case.

Evolution of the Near-Loss-Cone Distribution

Figure 2 shows the evolution of the distribution function from an initial loss-cone edge distribution (dashed curve in each panel). The bouncing resonant electrons can interact with the 3-s wave pulse near the equatorial region up to 4 times. The modified distributions are shown immediately after the particles cross the equatorial plane at six different times.

The first encounter of the distribution with the wave occurs at $t = t_w$. The modified distribution then arrives at the northern hemisphere (at 100 km) at $t = t_w + t_e$ where the number of particles that backscatter from the atmosphere is determined as described above with $\alpha = 90°$ corresponding to an equatorial pitch angle of $\alpha_{eq} = \alpha_{lc}^N = 13°$. The same distribution then reaches the low-altitude (100 km) southern hemisphere at $t = t_w + 3t_e$, where a similar process occurs but with $\alpha_{\text{local}} = 90°$ corresponding to $\alpha_{eq} = \alpha_{lc}^S = 15°$. The second equatorial encounter with the southgoing wave then occurs at $t = t_w + 4t_e$, and the distribution after this encounter is given in the second panel. Further scattering by the wave more than compensates for the particles lost during the previous atmospheric encounters so that the particle population for $\alpha \leq 13.6°$ is increased as more particles are scattered to lower pitch angles. The form of $f(v_{\|_{eq}}, \alpha_{eq})$ evolves along similar lines at times $t = t_w + 8t_e$ and $t = t_w + 12t_e$, but the situation changes after the time $t = t_P + t_w$ when the wave tail leaves the equator. No further wave-induced scattering occurs on equatorial transit at the times $t = t_w + 16t_e$ and $t = t_w + 20t_e$, and as a result the particle population in the pitch angle range $\alpha < \alpha_{lc}^S = 15°$ is gradually reduced during its successive encounters with the atmosphere.

In the following subsection we discuss the measurements of the near loss-cone edge distribution, which are used for selecting appropriate initial distributions for our analysis.

Measurement of the Loss-Cone Edge Distribution

While the trapped flux level for the local equivalent of $\alpha_{eq} > 13.6°$ was not accessible to the SEEP detectors at the time of the August 17, 1982, event, the differential fluxes near the loss cone were measured during the southern hemisphere transit across the L=2.3 shell. In these southern hemisphere passes near the longitude of NAA a 90° pitch angle at the satellite altitude corresponded to α_{eq} in the range of 15°-16°. An example of such measurements is shown in Figure 3, where the upper set of points show the differential energy spectrum (averaged over 1.98 seconds) measured on August 17, 1982, in the southern hemisphere using the detector with local zenith angle of 90°, which corresponds to an equatorial pitch angle $\alpha_{eq} \simeq 15.6°$. The lower points show the differential energy spectrum in the northern hemisphere during the time the fluxes were modulated by NAA. The same detector with a central zenith angle of 90° was used in this case, measuring particles with $\alpha_{eq} \leq 13.6°$.

Using data similar to those shown in Figure 3, from different passes of the SEEP satellite during the month of August, 1982 in a longitude range within ±5° that of the NAA transmitter, the range of flux values for 17.7 keV particles at L=2.3 were obtained. The results are shown in Figure 4, where the pluses and circles indicate the southern and northern hemisphere values respectively. The one data point representing the observation at the time of the August 17, 1982, event is indicated by a solid circle. The values shown in Figure 4 are obtained by averaging over periods of 8.19 seconds centered around the time of the satellite crossing of the $L = 2.3$ field line.

Also shown in Figure 4 are the four different loss-cone distributions (I, II and *a*, *b*) used in the next section for the computation of the time evolution of the electron flux. These distributions are selected to be in approximate agreement with the data points.

In deriving the differential energy spectra values shown with pluses or circles from measured counts, the pitch angle distribution across the angular range of the detector was taken to be given by I*a*.

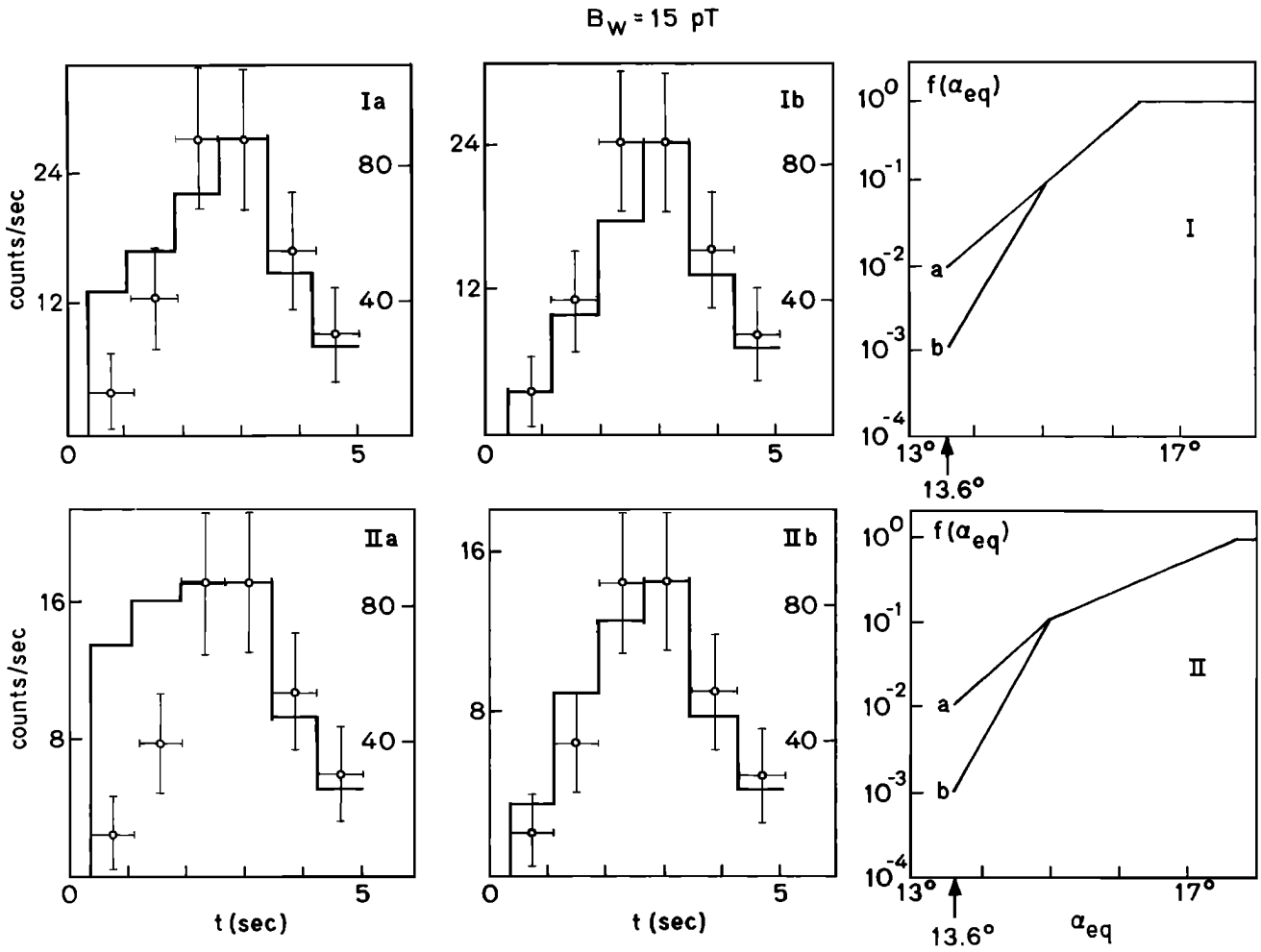

Fig. 5. The temporal variation of the computed and measured count rates for different loss-cone edge distributions I, II and *a*, *b* shown in the rightmost column. The measured points are shown with the corresponding uncertainty and represent averages over ~ 0.8 s, i.e., the time resolution of the model computations. The count rate scale for the measured profile is given on the right hand axis, while that for the computed profiles is shown on the left hand axis. The scale for the model results is adjusted to facilitate ready comparison of the computed and measured profiles. The different distribution functions are all normalized to the same level for $\alpha_{eq} = 18°$, corresponding to a differential energy spectrum of 7.5×10^3 el/cm^{-2} s^{-1} s^{-1} keV^{-1}.

Time Evolution of Electron Flux Observed at Satellite Altitude

The time dependence of the precipitation pulses expected for various kinds of initial near loss-cone distributions is shown in Figure 5. The different distributions considered are shown in the right hand column and are classified as I, II and *a*, *b*. The data points indicate the measured count rate of the SEEP detector pointed at 90° with respect to the zenith and is the energy range of 17.7±1.8 keV. The count rates given here correspond to the 3 s on/2 s off cycle that is closest to the satellite crossing of the $L = 2.3$ field line (~ 8720 seconds on August 17, 1982). The statistical errors in the measured count rates are shown with vertical error bars. Since the model calculations involve only particles in the range 17.7±1.8 keV interacting with the wave on the $L \simeq 2.3$ field line, the flux profile shown in Figure 5 is appropriate for comparison. The numbers given on the right hand axis of the panels *a*, *b* in Figure 5 are the absolute incremental count rates, representing the counts that are observed above a background that is assumed to have no effect on the determination of the temporal profile.

The solid lines in Figure 5 represent the computed count rate profiles, updated at discrete steps of $t = t_w + kt_e$, where $k = 1, 5, 9$, etc., represents successive encounters of the particle distribution with the SEEP satellite. The first four steps in each panel involve wave-induced scattering, whereas the last two steps represent the gradual reduction in the flux after the wave has left the magnetic equator as discussed in connection with Figure 2. The scale for the model results is in each case adjusted to facilitate comparison of the computed and measured temporal profiles. The absolute levels for the computed profiles are separately indicated on the left-hand axis. The various initial distributions used for comparison are all normalized to the same level at $\alpha_{eq} = 18°$, corresponding to a flux at this pitch angle for 17.7 keV electrons of 7.5×10^3 el cm^{-2} s^{-1} sr^{-1} keV^{-1}, as shown in Figure 4. The stepwise nature of the computed flux stems from the fact that our calculations apply to the scattering of particles representing the leading edge of a continuous distribution of electrons.

The results presented in Figure 5 indicate general agreement between the data and the model results as far as the temporal profile of the count rate is concerned. Of the four distributions used, I*b* and II*b* provide a better fit to the data. When the absolute peak count rates are considered I*b* is favored, but even that profile leads to a predicted rate which is somewhat lower than the measured rate.

Figure 6 shows the time profiles for a 30 pT equatorial wave magnetic field intensity and for the initial distributions of I*a* and *b*. The format of this figure is similar to that of Figure 5. It is seen from Figure 6 that the computed count rate profiles are relatively independent of the shape of the distribution in the range $\alpha < 15°$. This is because for $B_w = 30$ pT, single-encounter pitch angle changes can be as high as 2°, so that the particles observed by SEEP ($\alpha < 13.6°$) could have been scattered down from pitch angles $\alpha > 15°$ in a single encounter with the wave. By comparison, the maximum individual particle scattering for 15 pT is 1°. Each of the computed profiles of Figure 5 provides a reasonable fit to the data in terms of the temporal variation, and the peak computed count rates for 30 pT are higher than observed values.

It should be noted that even though individual particles can cross the gap in single encounters with the 30 pT wave, consideration of atmospheric backscatter and multiple interactions is still necessary to explain the observed temporal count rate profile. The only difference between the 15 pT and the 30 pT waves is that the latter precipitates more flux.

Precipitation at Higher Energies

Up to now we have considered an approximately monoenergetic stream of particles corresponding to the spectral peak energy of 17.7 keV observed by the SEEP detectors at L=2.3 on August 17, 1982. However, the modulated electron fluxes observed on this day involved electrons covering a range of energies up to 100 keV [*Imhof et al.*, 1983*a*].

For gyroresonant wave-particle interaction involving a longitudinally propagating wave and a resonant particle energy of 17.7 keV at the equator, the scattering of particles at higher energies is understood to be due to interactions

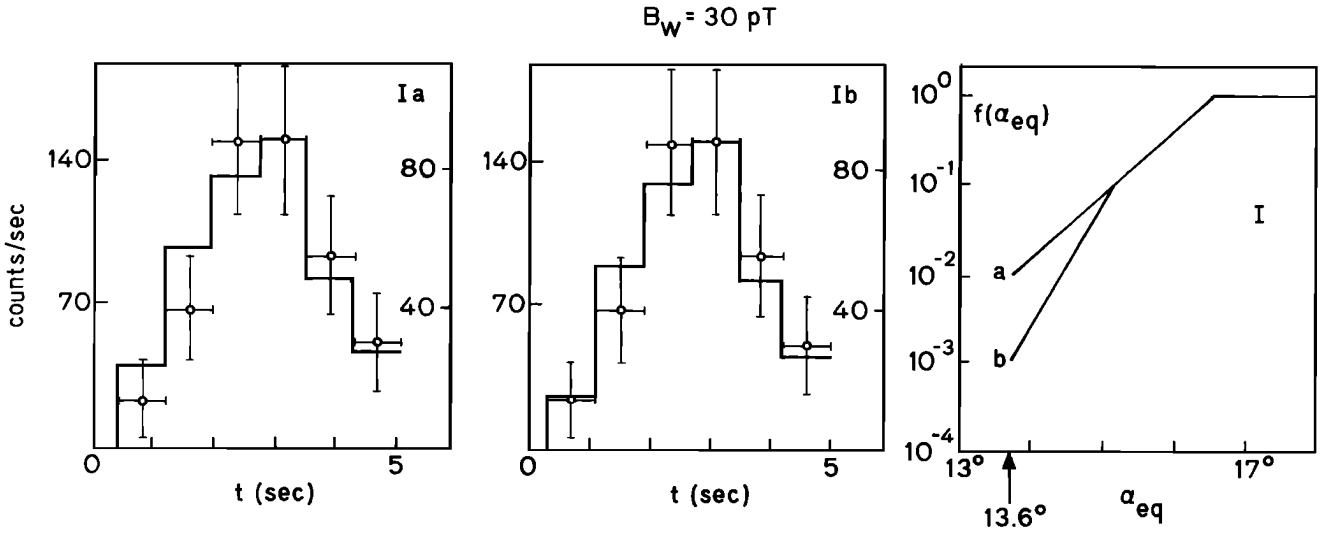

Fig. 6. Comparison of the measured and computed temporal count rate profiles for $B_w = 30$ pT. The format is the same as that of Figure 5 except that only the distributions I*a* and *b* are considered.

at locations off the magnetic equator, where the resonant particle energies as given by equation (A1) are higher. The spectral peak of 17.7 keV is attributed to equatorial interactions, since for longitudinally propagating waves, the largest particle scatterings occur at the magnetic equator [*Inan et al.*, 1978].

Figure 7 shows the computed count rate profile for particles in the energy range 45±1.8 keV. The initial loss-cone edge distribution for the case shown was assumed to be the Ia distribution of Figure 4. Because of the relatively low count rates at the higher energies, a comparison of this profile with data using the format of Figures 5 and 6 could not be made. In other words, the count rate statistics in a single energy channel having a width of 3.6 keV are not sufficient for defining a temporal profile. Thus, the lower panel of Figure 7 shows the measured count rate integrated over all energies above 45 keV but corresponding to the 3-s on/2-s off cycle starting at 8715 seconds ($L \simeq 2.3$) on August 17, 1982. We see from this result that the measured temporal count rate profile is similar to that at lower energies.

The computed profile, on the other hand, does not display the slow rise seen in the data. After the first scattering step, the particle distribution near the loss cone is reduced as a result of its successive encounters with the atmosphere, but the wave-induced scatterings are not large enough to compensate for this reduction. It should be noted that the individual particle scattering for 45 keV electrons is roughly an order of magnitude lower than for 17.7 keV energy. If particles with even higher energies than 45 keV are considered, the model result would be similar, since the fundamental mechanism for the interaction remains the same.

The difference between the model result and the observed count rate for higher energy particles can be attributed in part to our assumption that the cold plasma along the magnetic field lines is in diffusive equilibrium [*Angerami and Thomas*, 1964]. The cold plasma variation along the field lines determines the variation of the refractive index n, which in turn determines the length of the wave-particle interaction region through equation (A1) and therefore the magnitude of the individual particle scatterings. In a diffusive equilibrium model, the cold plasma density is nearly constant at latitudes close to the magnetic equator so that the interaction length is mainly determined by the variation of the electron gyrofrequency. The wave-induced pitch angle scatterings then become increasingly smaller at higher energies, involving interactions at higher latitudes where the gyrofrequency variation is more rapid. A cold plasma distribution that allows for a faster increase of density with distance from the equator would tend to compensate for the rapid variation of the electron gyrofrequency and would tend to increase the rms scattering at higher energies. Thus the data of August 17, 1982, may be indicative of a nondiffusive equilibrium variation of the cold plasma density. Another possibility is the presence of localized irregularities in density along the field lines which again could result in increased mean-square scattering.

Another reason for the difference between observed and computed flux profiles at high electron energy might be related to our assumption of longitudinal wave propagation with wave normal $\theta = 0°$, in contrast to evidence that the scattering waves may have propagated in the nonducted mode with $\theta > 0°$ (see appendix). While a formulation of the theoretical basis of interactions of obliquely propagating waves and particles has recently become available [*Bell*, 1984], no quantitative estimates exist for precipitation induced by such waves. In general, for nonducted interactions, the wave-induced scattering efficiency may be maximized at locations other than the magnetic equator, depending on the distribution of the ray paths and the variation of the wave normal along the ray path. Such effects may help to explain the discrepancy between the computed and observed flux profiles at higher energies and will be the subject of future work.

6. DISCUSSION

Wave Echoing and Reflection

While the slow rise and decay of the observed precipitation pulses may also be due to multiple bounces of the wave packet, this possibility seems unlikely for a number of reasons. Magnetospheric reflection of nonducted waves occurs near the point where the wave frequency is equal to the local lower hybrid resonance frequency [*Smith et al.*, 1964] which in the earth's magnetosphere is typically in the 4-15 kHz range. On this basis, reflection of a 17.8 kHz signal in this mode would not be expected. Also, nonducted rays originating in one hemisphere arrive at the other hemisphere with

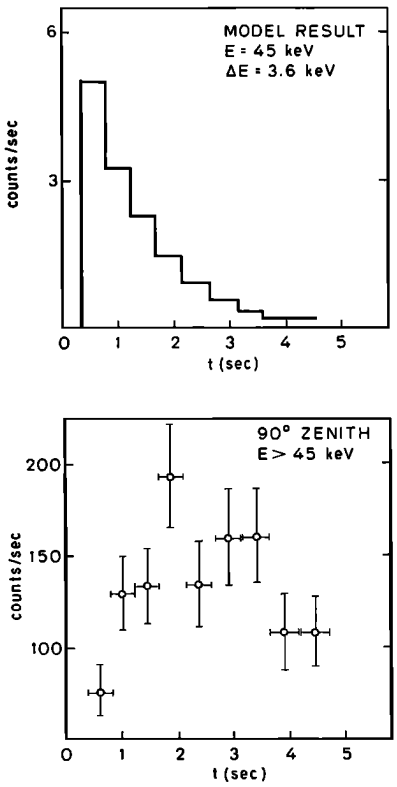

Fig. 7. The comparison of the measured and computed temporal profiles for particles with ~ 45 keV energy. The wave intensity was taken to be $B_w = 15$ pT, and loss cone distribution of Ia was assumed. The upper panel shows the computed profile for particles having energies of 45±1.8 keV, whereas the lower panel shows the count rate integrated over all energies >45 keV. The latter is done in order to improve on the limited count rate statistics for single energy channels.

very high wave normal angles $\theta \simeq \theta_r$, where θ_r is the resonance cone angle. While such signals can in principle reflect from the sharp lower boundary of the lower ionosphere, the high wave normals indicate that they will undergo significant absorption in the ionosphere before and after reflection [*Helliwell*, 1965]. Large scale density structures (such as a secondary plasmapause at L ~2.4) could guide 17.8 kHz waves between hemispheres and allow for reflection; however no independent evidence for such a condition exists. Thus, wave reflection and echoing seem to be an unlikely possibility for the August 17, 1982, case.

Wave Growth and Amplification

Our test-particle approach for computing the wave-induced particle scatterings inherently assumes that the individual particles move into the loss cone independently, i.e., that the particles do not interact with each other through the growth or amplification of the wave during the interaction. In the absence of wave measurements such wave-growth effects cannot be ruled out; however, as discussed in our previous work [*Inan et al.*, 1982] they can be approximately taken into account by considering a spatial wave structure having an increase in intensity beyond the equator. Calculations using such spatial wave intensity distributions indicate that the precipitation fluxes would not be appreciably different [*Inan et al.*, 1978]. It should also be noted that if wave growth were to occur, it is likely to be due to particles at higher pitch angles than those near the loss cone [*Helliwell*, 1967].

Note that while the kinematic aspects such as the electron and wave travel times do control the shape of the computed time profile to some degree, the absolute values of the scattering coefficients determine whether or not the wave-induced flux can be high enough to sustain an increase in spite of the partial loss of particles during ionospheric encounters twice every bounce period. If this were not the case (i.e., the scattering coefficients were not large enough) the computed flux would not show a stepwise increase in time. This fact and the close agreement between the computed and observed peak absolute count rates supports the mechanism of scattering considered here.

Measurement of Trapped Flux

An important factor in our comparisons of measured flux levels with computed count rates is the lack of measurements of the trapped flux for $\alpha_{eq} > 13.6°$ at the time of the observations of the modulated precipitation events. Simultaneous measurement of the trapped and precipitating flux levels would have been valuable in more accurately defining the loss-cone edge distribution and thus providing an initial pitch angle distribution for the calculations. This situation is an inherent limitation of observations carried out on low altitude satellites. The results presented in this paper illustrate the importance of the details of the loss-cone profile in determining the precipitation flux levels. In order to measure such features, high resolution pitch-angle measurements ($< 2°$) should be made on satellites that cross the magnetic equatorial plane over L shells 2-5.

L Range of Observations

We have limited our modeling to the observations made at $L \simeq 2.3$, although the L range of the August 17, 1982, observations extended from L =2.1 to 2.4. The peak energy of the observed flux decreased with increasing L, and was as high as ~30 keV at $L \simeq 2.1$. Since the bounce period of these resonant particles is ~30% shorter than that of 17.7 keV particles at L=2.3, they can undergo five interactions with the wave near the equatorial plane. In the context of the model presented here, the computed count rates of Figure 4 would reach a maximum in five (instead of four) steps and would decay in three (instead of two) steps, with no fundamental difference in the basic physical mechanism involved.

The slow increase in the peak count rate by a factor of ~4 between L=2.1 and L=2.3 [*Imhof et al.*, 1983*a*] may be due to (1) increased wave signal intensity as the distance to the source is decreased, (2) the fact that the scattering efficiency of the wave particle interaction increases with L [*Inan et al.*, 1982] or (3) increased trapped flux level at higher L.

An important feature of the SEEP observations on August 17, 1982 is the relatively abrupt decrease in the flux level for L >2.4, in spite of the fact that the source of the wave energy, the NAA transmitter, is located at $L \simeq 3$. The data presented in Figure A2 indicate that this decrease is not due to the ~6 keV detection threshold of the SEEP instruments. Factors that can directly account for the observed decrease at $L > 2.4$ are variations in the trapped flux level as a function of L and cold plasma density irregularities that may defocus the wave energy at low altitudes. While no measurements of the former were available, traveling ionospheric disturbances (TID's) were detected by the Langmuir probe instrument on the SEEP satellite during the time of the August 17, 1982, pass [*Voss et al.*, 1984]. These TID's involve horizontal gradients that could defocus the waves and hence reduce their intensity.

7. SUMMARY AND CONCLUSIONS

Many features of the transmitter-induced electron precipitation events observed by the SEEP satellite detectors can be understood through a straightforward application and extension of existing models of the wave-induced particle precipitation process [*Inan et al.*, 1982]. In applying the model one needs to consider the pitch angle dependence of the electron distribution function near the loss cone as well as atmospheric backscatter of electrons and multiple interactions of particles with the wave. Such aspects of the wave-induced precipitation process have not been studied in detail in previous work, which has mainly dealt with the first order wave-particle scattering under idealized conditions (e.g. symmetrical loss cone angles for both hemispheres).

While several features of the observations were found to be consistent with model predictions, there are important differences between the measured and computed count rate profiles for higher energy particles as discussed in connection with Figure 7. The reasons for these discrepancies are not understood but may be due to deviations from a simple diffusive equilibrium model of the background cold plasma density along the magnetic field lines or to the nonducted nature of the waves.

Finally, we note here that the model that has been found to agree with several features of the August 17, 1982, data would be expected to apply to the other cases of VLF transmitter induced precipitation events observed by SEEP

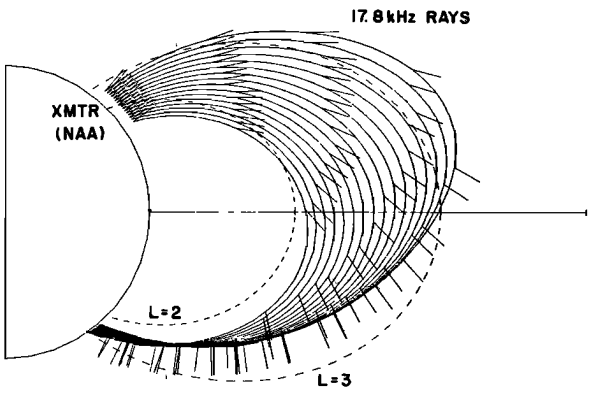

Fig. A1. Ray paths for 17.8 kHz signals for a cold plasma density profile that is proportional to r^{-4}, where r is the radial distance. The signals are injected with vertical wave normal angles in the northern hemisphere. The short bars indicate the local wave normal directions at various points.

[*Imhof et al.*, 1983b], since these were found to have similar properties in terms of L range of observations, temporal pulse shape and energy spectra.

8. Appendix: Wave Characteristics

Propagation Mode

As stated in section 2 above, the variation of the energy of the observed narrow peaks on August 17, 1982, was found to be consistent with an L^{-4} dependence of n_{eq} for assumed scattering near or at the equatorial plane by waves propagating with wave normals $\theta \simeq 0°$ [*Imhof et al.*, 1983*a*].

In general, whistler mode waves propagate in the magnetosphere in the nonducted mode for which the wave normal angle θ is not necessarily small. Examples of ray paths for 17.8 kHz rays are shown in Figure A1, for uniformly distributed points of injection at 500 km altitude with wave-normal angles initially aligned with the local vertical. For the rays shown in Figure A1 a diffusive equilibrium model for the cold plasma density [*Angerami and Thomas*, 1964] was used together with a centered dipole model of the earth's magnetic field.

In order to determine whether the observed narrow spectral peaks correspond to interactions with ducted or nonducted waves we consider the cyclotron resonant condition,

$$\omega + \frac{n\omega}{c} v_R \cos\theta \simeq \omega_H \qquad \text{(A1)}$$

where n is the whistler mode refractive index and is a function of wave frequency, wave normal angle θ, cold plasma density and gyrofrequency ω_H and v_R is the particle resonant velocity. Since the refractive index is a function of the cold plasma density, an independent measurement of cold plasma density is needed in order to compare the v_R (or E_R) values computed from (A1) with the measured values.

To estimate the equatorial cold plasma density n_{eq}, we have used broadband VLF recordings made at Siple Station, Antarctica, during the time of the August 17, 1982, observations. Repeated measurements of the nose frequency and nose travel time of a whistler element observed in the Siple data were utilized in the whistler-dispersion method for determining the equatorial cold plasma density and the field line of propagation [*Park*, 1972]. The cold plasma density at $L \simeq 2.89$ at the time of the SEEP observations was found to be $n_{eq} = 785 \pm 75$ el/cm^3. In order to determine the cold plasma density at other L values we adopt a model for the variation of n_{eq} with L. In the following we give results for n_{eq} proportional to L^{-4} and L^{-5}.

Figure A2 shows the variation of the equatorial resonant energy E_R, computed from (A1), for wave normals $\theta_{eq} = 0°, 30°, 60°$, wave frequency $f = 17.8$ kHz and n_{eq}=785 el/cm^3 at $L = 2.89$. The solid lines are for the case where n_{eq} was assumed to vary as L^{-4}, whereas the dashed lines are for L^{-5}. The separate points indicated with a plus in Figure A2 are the measured energies of the spectral peaks observed with the SEEP detectors [*Imhof et al.*, 1983*a*].

The observed variation of E_R with L is consistent with either (1) an L^{-4} dependence of n_{eq} for an equatorial wave-normal angle $\theta_{eq} \simeq 30°$ or (2) an L^{-5} dependence of n_{eq} for $\theta_{eq} \simeq 60°$. The equatorial wave-normal angles for the raypaths of Figure A1 are in the range $\theta_{eq} \simeq 40°$-$50°$, in general agreement with these estimates. However, given the 10% uncertainty in the measured value of n_{eq} at $L = 2.89$, a wave normal of $\theta \simeq 0°$ cannot be ruled out on the basis of the results given in Figure A2. Other evidence, such as the observation of modulated precipitation pulses over an L range of 2.1 to 2.4, indicates that the waves probably propagated in the nonducted mode. This argument is based on the belief that the typical dimensions of whistler mode ducts are less than $\sim 0.1L$ at the equatorial plane [*Angerami*, 1970].

Thus we conclude that the value of n_{eq} obtained via an independent measurement using whistlers observed at Siple Station, Antarctica, is consistent with the L-dependent variation of the energies of the narrow spectral peaks observed by the SEEP detectors on August 17, 1982. This conclusion is based on the assumption that the observed peaks were caused by interactions near the geomagnetic equator with monochromatic waves having a frequency of 17.8 kHz and propagating in the nonducted mode with wave normals $\theta_{eq} = 30°$–$60°$.

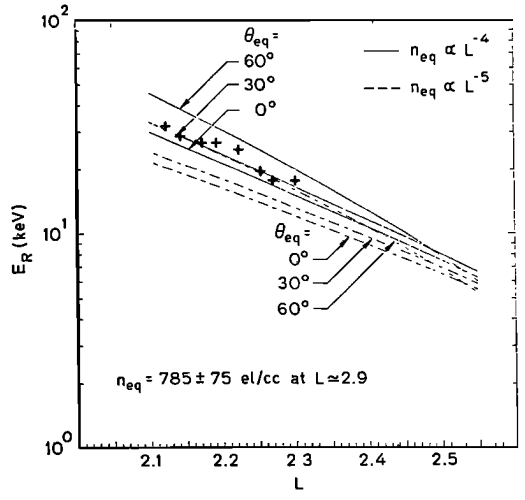

Fig. A2. The equatorial resonant particle energy E_R computed from (A1) and plotted versus L for various θ_{eq}. The solid lines are for the case with n_{eq} proportional to L^{-4}, whereas the dotted lines are for n_{eq} proportional to L^{-5}.

Travel Time to the Equator

The group travel time for 17.8 kHz signals from the ionosphere to the equatorial plane at L=2.3 for the ray paths shown in Figure A1 and for $n_{eq} \simeq 2458$ el/cm^3 (as obtained by using n_{eq} proportional to L^{-5} and $n_{eq} = 785$ el/cm^3 at $L \simeq 2.89$) is found to be $t_w \simeq 0.4$ s. For ducted propagation (as assumed in the model calculations presented in this paper) and with $n_{eq} \simeq 1585$ el/cm^3 (so that $E_R = 17.7$ keV at L=2.3 for 17.8 kHz) the group time delay is lower, with $t_w = 0.2$ s. The difference between ducted and nonducted time delays is smaller than the particle bounce period and is thus insignificant for the purposes of the model calculations reported here.

Wave Magnetic Field Intensity

The wave-induced scattering results given in this paper are dependent on the equatorial wave magnetic field intensity. While no independent measurement of the wave characteristics during the August 17, 1982, event was available, a simplified model can be used to estimate the wave power density at the equatorial plane [*Inan et al.*, 1984].

The radiated power of the NAA transmitter operating at 17.8 kHz is taken to be 1 megawatt [*Inan et al.*, 1984]. The losses in the earth ionosphere waveguide between the transmitter and the point of entry of the wave into the magnetosphere ($L \simeq 2.3$) and the absorption and polarization losses in the nighttime ionospheric D region can be accounted for roughly within an uncertainty of ±5 dB [*Helliwell*, 1965]. If we further assume ducting in the magnetosphere we can map the wave power up to the equatorial plane in accordance with the divergence of the magnetic field lines. Then, including the changing refractive index, we find an equatorial B_w=10.3 pT for n_{eq}=1585 el/cm^3 and for a wave normal of $\theta = 0°$. However, considering nonducted ray paths similar to those shown in Figure A1, the divergence loss is less, leading to an estimated value of ~20 pT for the same n_{eq} and θ. If we further account for the nonzero wave normal angle and use θ =40°-50° and $n_{eq} \simeq$2200 el/cm^3 (so as to be consistent with an equatorial E_R=17.7 keV) for computing the local refractive index we find $B_w \simeq$30 pT.

On this basis, and in view of the uncertainties in these approximate estimates, we have chosen to do our calculations in this paper using two representative wave magnetic intensities, namely 15 and 30 pT.

Acknowledgments. Special acknowledgment is made of the role played by R. G. Joiner of the Office of Naval Research (ONR) in the successful management and coordination of the various elements of the SEEP program. We appreciate the discussions we have had with our colleagues at the STAR Lab of Stanford University and at the Lockheed Palo Alto Research Labs (LPARL). We thank J. P. Katsufrakis for his contributions in the coordination of the Stanford portion of SEEP experiments, and D. L. Carpenter for his help in the scaling of the whistlers received at Siple Station. The contributions of H. D. Voss, E. E. Gaines and D. Datlowe of the LPARL were essential to the electron measurements used in this paper. The Stanford University effort for this work was supported under (ONR) grant N00014-82-K-0489. The Siple Station data used in the appendix were acquired under support from the Division of Polar Programs of the National Science Foundation under grant NSF-80-22282. The work at LPARL was supported by ONR contract N00014-79-C-0824 and orbital support was provided by the Air Force Space Test Program Office. The development of the test particle model used extensively in this paper was originally supported by the National Aeronautics and Space Administration under contract NGL-05-020-008. In carrying out the computations reported in this paper we have made use of a computer time grant from the National Center for Atmospheric Research (NCAR) and have utilized the NCAR computer facilities in Boulder, Colorado

The Editor thanks S. A. Curtis and another referee for their assistance in evaluating this paper

REFERENCES

Angerami, J. J., Whistler duct properties deduced from VLF observations made with the OGO-3 satellite near the magnetic equator, *J. Geophys. Res., 75*, 6115, 1970.

Angerami, J. J., and J. O. Thomas, Studies of planetary atmosphere, 1, The distribution of electrons and ions in the earth's exosphere, *J. Geophys. Res., 69*, 4537, 1964.

Arnoldy, R. L., K. Dragoon, L. J. Cahill, Jr., S. B. Mende, T. J. Rosenberg, and L. J. Lanzerotti, Detailed correlation of magnetic field and riometer observations at L=4.2 with pulsating aurora, *J. Geophys. Res., 87*, 10449, 1982.

Bell, T. F., The nonlinear gyroresonance interaction between energetic electrons and coherent VLF waves propagating in an arbitrary angle with respect to the earth's magnetic field, *J. Geophys. Res., 89*, 905, 1984.

Bell, T. F., U. S. Inan, and R. A. Helliwell, Nonducted coherent VLF waves and associated triggered emissions observed on the ISEE-1 satellite, *J. Geophys. Res., 86*, 4649, 1981.

Berger, M. J., S. M. Seltzer, and K. Maeda, Some new results on electron transport in the atmosphere, *J. Atmos. Terr. Phys., 36*, 591, 1974.

Chang, H. C., and U. S. Inan, A theoretical model study of observed correlations between whistler mode waves and energetic electron precipitation events in the magnetosphere, *J. Geophys. Res., 88*, (A12), 10,053, 1983.

Davidson, G., and M. Walt, Loss cone distributions of radiation belt electrons, *J. Geophys. Res., 82*, 48, 1977.

Dingle, B., and D. L. Carpenter, Electron precipitation induced by VLF noise bursts at the plasmapause and detected at conjugate ground stations, *J. Geophys. Res., 86*, 4597, 1981.

Goldberg, R. A., S. A. Curtis, J. R. Barcus, C. L. Siefring and M. C. Kelley, Controlled stimulation of magnetospheric electrons by radio waves: experimental model for lightning effects, *Science, 219*, 1324, 1983.

Helliwell, R. A., *Whistlers and Related Ionospheric Phenomena*, Stanford University Press, Stanford, Calif., 1965.

Helliwell, R. A., A theory of discrete VLF wave emissions from the magnetosphere, *J. Geophys. Res., 72*, 4773, 1967.

Helliwell, R. A., J. P. Katsufrakis, and M. L. Trimpi, Whistler-induced amplitude perturbation in VLF propagation, *J. Geophys. Res., 78*, 4679, 1973.

Helliwell, R. A., S. B. Mende, J. H. Doolittle, W. C. Armstrong, and D. L. Carpenter, Correlations between λ4278 optical emissions and VLF wave events observed at L~ 4 in the Antarctic, *J. Geophys. Res., 85*, 3376, 1980.

Imhof, W. L., E. E. Gaines, and J. B. Reagan, Evidence for the resonance precipitation of energetic electrons from the slot region of the radiation belts, *J. Geophys. Res., 79*, 3141, 1974.

Imhof, W. L., R. R. Anderson, J. B. Reagan, and E. E. Gaines, The significance of VLF transmitters in the precipitation of inner belt electrons, *J. Geophys. Res., 86*, 11,225, 1981.

Imhof, W. L., J. B. Reagan, H. D. Voss, E. E. Gaines, D. W. Datlowe, J. Mobilia, R. A. Helliwell, U. S. Inan, and J. P. Katsufrakis, Direct observation of radiation belt electrons precipitated by the controlled injection of VLF signals from a ground-based transmitter, *Geophys. Res. Lett., 10*, 361, 1983*a*.

Imhof, W. L., J. B. Reagan, H. D. Voss, E. E. Gaines, D. W. Datlowe, J. Mobilia, R. A. Helliwell, U. S. Inan, and J. Katsufrakis, The modulated precipitation of radiation belt electrons by controlled signals from VLF transmitters, *Geophys. Res. Lett., 10*, 615, 1983*b*.

Inan, U. S., T. F. Bell, and R. A. Helliwell, Nonlinear pitch angle scattering of energetic electrons by coherent VLF waves in the magnetosphere, *J. Geophys. Res., 83*, 3235, 1978.

Inan, U. S., T. F. Bell, and H. C. Chang, Particle precipitation induced by short-duration VLF waves in the magnetosphere, *J. Geophys. Res., 87*, 6243, 1982.

Inan, U. S., H. C. Chang, and R. A. Helliwell, Electron precipitation zones around major ground-based VLF signal sources, *J. Geophys. Res., 89*, 2891, 1984.

Koons, H. C., B. C. Edgar, and A. L. Vampola, Precipitation of inner zone electrons by whistler mode waves from the VLF ransmitter UMS and NWC, *J. Geophys. Res., 86,* 640, 1981.

Larsen, T. R., T. A. Potemra, W. L. Imhof and J. B. Reagan, Energetic electron precipitation and VLF phase disturbances at middle latitudes following the magnetic storm of December 16, 1971, *J. Geophys. Res., 82,* 1519, 1977.

Olson, W. P., K. A. Pfitzer, and G. J. Mroz, Modeling the magnetospheric magnetic field, in *Quantitatwe Modelng of Magnetospheric Processes* Geophys. Monogr. Ser., vol. 21, edited by W. P. Olson, pp. 77-85, AGU, Washington, D. C. 1979.

Park, C. G., Methods of determining electron concentrations in the magnetosphere from nose whistlers, *Tech. Rep. 3454-1,* Radiosci. Lab., Stanford Electron. Lab., Stanford Univ., Stanford, Calif., 1972.

Rosenberg, T. J., R. A. Helliwell, and J. P. Katsufrakis, Electron precipitation associated with discrete very-low-frequency emissions, *J. Geophys. Res., 76,* 8445, 1971.

Smith, R. L., N. Brice, J. Katsufrakis, D. A. Gurnett, S. D. Shawhan, J. S. Belrose, and R. E. Barrington, An ion gyrofrequency phenomenon observed in satellites, *Nature, 204,* (4955), 274, 1964.

Stadsnes, J., and B. Maehlum, Scattering and absorption of fast electrons in the upper atmosphere, internal report, Norw. Def. Res. Estab., Kjeller, Norway, 1965.

Vampola, A. L., and G. A. Kuck, Induced precipitation of inner zone electrons, 1, Observations, *J. Geophys. Res., 83,* 2543, 1978.

Voss, H. D., W. L. Imhof, J. B. Reagan, K. L. Miller, and J. Mobilia, TID's above thunderstorms associated with the efficient transmission of VLF energy through the ionosphere, (abstract), *Eos Trans. AGU, 65,* 267, 1984.

H. C. Chang, R. A. Helliwell, and U. S. Inan, STAR Laboratory, Stanford University, Stanford, CA 94305.

W. L. Imhof, J. B. Reagan, and M. Walt, Lockheed Palo Alto Research Laboratory, Palo Alto, CA 94304.

(Received May 14, 1984;
revised August 13, 1984;
accepted August 28, 1984.)